density. Therefore, the intensity of magnetic neutron diffraction peaks falls off much more rapidly with $(\sin\theta)/\lambda$ than do nuclear neutron diffraction peaks.

3.2.2.3. *Peak shapes*

The shape of a powder-diffraction peak is a convolution of the intrinsic line shape due to the microscopic structure of the sample crystallites (*e.g.* size and strain) and the configuration of the instrument used to record the pattern. A major goal of powder-diffraction analysis is to be able to separate the contributions of instrument and sample, so that information about the microstructure of the sample can be extracted reliably. On the other hand, in some cases one simply wants to be able to model the combined influence of instrument and sample, to obtain a functional form that permits the most accurate way of apportioning intensities to partially overlapping peaks.

Consider first the sample-dependent factors. The following division into size and strain effects is somewhat artificial, insofar as lattice strains affect the size of the coherently diffracting domain. Nevertheless, it is common to make a distinction between the two, as size broadening produces a peak width proportional to $1/\cos\theta$ in angle-dispersive measurements, whereas the peak width is proportional to $\tan\theta$ for strain broadening.

3.2.2.3.1. *Domain size*

In very general terms, diffraction peaks from an object of linear size L will have a width in Q of the order of $1/L$. As formulated by Scherrer (1918), in an angle-dispersive measurement, the full width at half-maximum (FWHM) in 2θ, measured in radians, is given by

$$\Gamma = \frac{K\lambda}{L\cos\theta}, \tag{3.2.12}$$

where K is called the shape factor and is a number of the order of unity whose precise value depends on the shape of the particles, which are assumed to be of uniform size and shape. The FWHM shape factor for a spherical particle is $K = 0.829$ (Patterson, 1939). Note that if a powder sample is polydisperse (*i.e.*, it contains a distribution of grain sizes), the average grain size is not necessarily given by the Scherrer equation.

Perhaps a more useful measure of the width of a peak is the integral breadth. In an angle-dispersive measurement, the integral breadth of a given peak centred at $2\theta_0$ is defined as

$$\beta = \frac{1}{I(2\theta_0)}\int I(2\theta)\,\mathrm{d}2\theta.$$

From a technical point of view, measurement of the integral breadth requires accurate measurement of the intensity in the wings of the diffraction peak, which in turn depends on accurate knowledge of the background intensity.

For any crystallite shape, it can be shown that the integral breadth is related to the volume-average thickness of the crystallite in the direction of the diffraction vector, *viz.*

$$L_V = \frac{\lambda}{\beta\cos\theta} = \frac{1}{V}\int \mathrm{d}^3\mathbf{r}\,T(\mathbf{r},\mathbf{G}),$$

where V is the volume of the crystallite and $T(\mathbf{r},\mathbf{G})$ is the length of the line inside the crystallite parallel to $\mathbf{G}$ and passing through the point $\mathbf{r}$. For example, if one writes an integral-breadth version of the Scherrer equation,

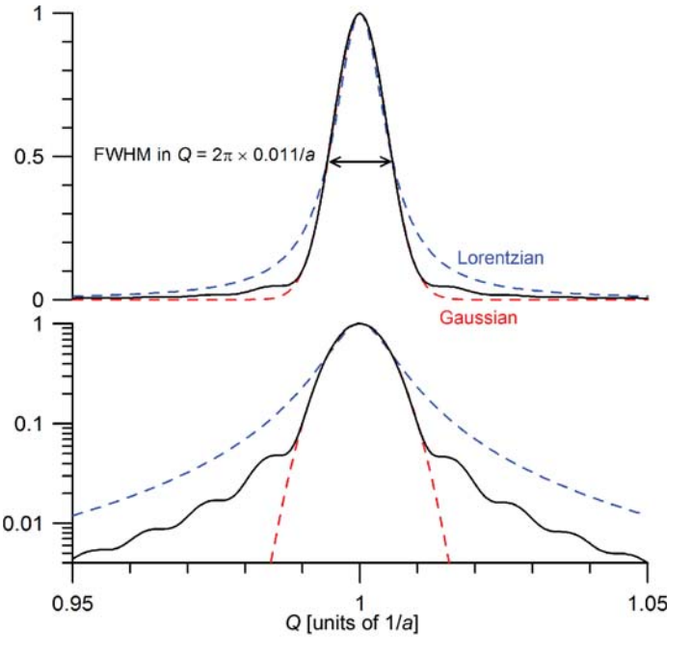

Figure 3.2.1
Computed powder line shape from an ensemble of spherical particles of diameter $100a$, including comparison to Gaussian and Lorentzian line shapes of equal FWHM.

$$\beta = \frac{K_\beta\lambda}{L\cos\theta},$$

the shape factor K_β is unity for $(00l)$ reflections from cube-shaped crystals of size L. $K_\beta = 1.075$ for a sphere of diameter L.

An important feature of the integral breadth is that it has a well defined meaning for a polydisperse sample of crystallites. Assuming that the crystallites all have the same shape,

$$\beta = \frac{K_\beta\lambda\langle L^3\rangle}{\cos\theta\langle L^4\rangle},$$

where $\langle L^3\rangle$ and $\langle L^4\rangle$ are the third and fourth moments of the size distribution (Langford & Wilson, 1978).

In many applications such as Rietveld or profile refinement, it is important to treat the full shape of the diffraction peak instead of merely its width (Loopstra & Rietveld, 1969; Rietveld, 1969). By way of illustration, Fig. 3.2.1 shows one Bragg peak of the computed powder-diffraction pattern from an ensemble of spherical particles of point scatterers in a simple cubic lattice. The lattice parameter is a, and the diameter of the particles is chosen to be $100a$, so that each crystallite consists of approximately 5.2×10^5 'atoms'. (This line shape was calculated using the Debye equation, described in Section 3.2.4.)

Several different analytical functions are frequently used in powder diffraction. In terms of the independent variable x, centred at x_0 with FWHM Γ, the normalized Gaussian function is

$$G(x-x_0) = \pi^{-1/2}\sigma^{-1}\exp-\left(\frac{x-x_0}{\sigma}\right)^2,$$

with $\sigma = \Gamma/2(\ln 2)^{1/2}$. The normalized Lorentzian is

$$L(x-x_0) = \frac{\Gamma/2\pi}{(x-x_0)^2+(\Gamma/2)^2}.$$

The symmetric Pearson-VII function is a generalization of the Lorentzian, written as

$$P(x - x_0) = \frac{a}{\Gamma}\left[1 + b\left(\frac{x - x_0}{\Gamma}\right)^2\right]^{-m}.$$

Here m is a parameter that governs the line shape (essentially the strength of the wings *versus* the peak), and the numerical parameters $b = 4(2^{1/m} - 1)$ and $a = (b/\pi)^{1/2}\Gamma(m)/\Gamma(m - 1/2)$. (Note the gamma function in the definition of a; the FWHM does not appear in that expression.) The Pearson-VII function with $m = 1$ is a Lorentzian, and it is a Gaussian in the limit $m \rightarrow \infty$.

It must be emphasized that none of these functions has any theoretical justification whatsoever. However, in loose powders size broadening is almost always Lorentzian, while Gaussian size broadening is more commonly observed in dense polycrystalline specimens (such as bulk metals).

The Lorentzian and Gaussian functions are also plotted in the same figure for comparison to the actual powder-diffraction line shape of a spherical particle. It can be seen that the correct function has stronger tails than the Gaussian, but the Lorentzian line shape seriously overestimates the intensity in the wings. Both the Gaussian and the Pearson VII fail to capture the general feature that any compact object with a sharp boundary will give a diffraction line shape with tails that asymptotically decay as $(x - x_0)^{-2}$.

One approach to obtaining a more accurate phenomenological description to diffraction line shapes is the Voigt function, which is a convolution of a Gaussian and Lorentzian,

$$V(x - x_0) = \int \mathrm{d}x'\, G(x' - x_0)L(x - x').$$

The presence of two shape parameters, the independent widths of the Gaussian and Lorentzian functions, provide independent parameters to control the width and the strength of the wings in the Voigt line shape. The Voigt is more computationally expensive than any elementary function, and so a commonly used approximation is the pseudo-Voigt,

$$\mathrm{PV}(x - x_0; \Gamma) = \eta L(x - x_0; \Gamma) + (1 - \eta)G(x - x_0; \Gamma),$$

which is a mixture of Gaussian and Lorentzian functions of the same width. The parameter η controls the shape (strength of the wings) of the pseudo-Voigt line-shape function, independent of its width. There is a computationally convenient approximate relation between Voigt line-shape parameters Γ_L and Γ_G and the pseudo-Voigt Γ and η (Thompson *et al.*, 1987).

3.2.2.3.2. *Strain*

An individual crystal in a sample may be subject to lattice deformation, either due to forces external to that crystal, or to internal factors such as substitutional disorder and dislocations. A comprehensive treatment of microstructural properties and their effects on powder-diffraction peak shapes is given in Chapter 3.6 of this volume; this section gives a general overview from a phenomenological basis.

The simplest description of strain broadening imagines an ensemble of independent crystallites with different lattice parameters. If the crystallites have an isometric distribution of lattice parameters with a fractional width $\delta a/a$, that will be reflected in the range of d-spacings for each reflection. In an angle-dispersive measurement, this will lead to an angular width $\delta 2\theta = 2 \tan\theta\, \delta a/a$ (radians).

Physically plausible mechanisms for a distribution of strains in a powder sample include random inter-grain forces arising during crystallization and the elastic response to internal defects such as dislocations. In practice, these effects often give rise to peak widths which likewise grow as $\tan\theta$. However, there is no *a priori* basis for expecting any particular functional form for that distribution. Frequent practice is to assume a Gaussian, Lorentzian, Voigt, or pseudo-Voigt form for an isotropic strain broadening, with an adjustable parameter ε representing the FWHM of the strain distribution. The FWHM Γ of the chosen functional form is then $\Gamma_{2\theta} = 2\varepsilon \tan\theta$ for angle-dispersive measurements, $\Gamma_E = \varepsilon E$ for energy-dispersive X-ray measurements and $\Gamma_t = \varepsilon t$ for neutron time-of-flight measurements.

3.2.2.3.3. *Instrumental contributions*

The instrument used to collect diffraction data affects the observed line shape in many ways. A complete discussion is beyond the scope of this article (but see Chapter 3.1, and would have to consider many different diffraction geometries separately. One approach, generally known as fundamental parameters, is to model the effect of every optical element on the peak shape. The instrumental response function is then the convolution of all of these individual contributions.

The simplest (and most widely successful) application of fundamental parameters arises from the analysis of Caglioti *et al.* (1958, 1960) on the instrument response function of a step-scanning powder diffractometer at a reactor neutron source. Neutrons pass through a parallel-blade collimator to a monochromator crystal, through a second collimator to the sample, and then through a third collimator into the detector. It is a fair approximation to assume that the transmission functions of the collimators and the mosaicity of the monochromator are all Gaussians. In that case, the instrument response function produces diffraction peaks which are also Gaussians, with a width that depends on the diffraction angle as

$$\Gamma = \left(U \tan^2\theta + V \tan\theta + W\right)^{1/2}, \qquad (3.2.13)$$

where the parameters U, V and W can be expressed in closed form as functions of the collimator acceptances and monochromator angle and mosaicity (Caglioti *et al.*, 1958, 1960). Indeed, it was this simple form of the line-shape function that allowed Rietveld and co-workers to develop the important methodology of data analysis commonly known as the Rietveld or profile method (Loopstra & Rietveld, 1969; Rietveld, 1969).

The functional form used to describe the shape of the pulse that emerges from the moderator of a spallation neutron source, and the numerical values of the parameters which go into it, determine the peak shapes observed in the powder diffractometer at such an instrument. The treatment of such matters lies beyond this introduction; documentation of the widely used *GSAS* software includes a detailed description (Larson & Von Dreele, 2004; see also Chapter 3.3).

Analytical treatment of the resolution of X-ray diffractometers is generally complicated by the fact that the various contributions are more difficult to model, especially in the case of the para-focusing Bragg–Brentano geometry most commonly used in laboratory X-ray diffractometers. In the diffractometer, one generally considers factors that affect the line shape separately in the equatorial plane (the plane containing the source, sample and detector) and the axial direction (perpendicular to the equatorial plane, *i.e.*, parallel to the diffractometer axis). In the equatorial plane the resolution is primarily governed by the divergence of the X-ray beam illuminating the sample and by the width of the receiving slit, but there are numerous contributions to the diffraction peak width and shape from such factors as non-conformance of the flat sample surface to the focusing circle,

partial transparency of the sample and misalignment of the diffractometer (Cheary & Coelho, 1992). Even if a monochromator is used to select only the $K\alpha_1$ line, the radiation spectrum from an X-ray tube consists of several Lorentzian functions owing to satellite transitions.

Axial divergence produces a pronounced asymmetry of low-angle diffraction peaks to the low-angle direction (and on the high-angle side of peaks with 2θ near 180°). If the incident or diffracted rays are out of the equatorial plane, they will be intercepted at a detector setting below (above) the actual diffraction angle if it is small (close to 180°), respectively. The effect can be minimized, but not completely eliminated, by narrowing the beam-defining apertures in the equatorial direction, or by introduction of parallel-blade Soller (1924) slits. The full treatment of the effect of axial divergence in a Bragg–Brentano diffractometer has been presented in a computationally convenient form (Cheary & Coelho, 1998).

It is generally easier to model the instrumental response function of a powder X-ray diffractometer based on a synchrotron-radiation source with an analyser crystal, because the transfer functions of the various optical elements are simpler to express. One approach is to approximate the wavelength- and angle-dependent reflectivity of monochromator and analyser crystals by Gaussians, and derive a closed-form expression for the width of the instrument response function (Sabine, 1987). This has been extended to include collimating and focusing (in the scattering plane) mirrors (Gozzo *et al.*, 2006); see Chapter 3.1 for a full description of the relevant optical configurations. A shortcoming of this analytical approach is that the correct single-crystal reflectivity function is not a Gaussian, so it cannot account for the correct line shape, only provide an estimate of its width. Numerical convolutions to accurately model the line-shape function have been performed, and produce excellent agreement with measured profiles (Masson *et al.*, 2003).

Instead of the analytical approach described in the previous few paragraphs, one frequently writes a parametrized function for the measured line shape without concern for the connection between the numerical values of the parameters and the microscopic properties of the sample or the geometry of the diffractometer. For example, one can use the Caglioti form for diffraction peak width [equation (3.2.13)] on any diffractometer, and adjust the parameters U, V and W to some measured standard sample. If size and strain contributions to sample-dependent broadening are both regarded as Lorentzians, they could be combined as $\Gamma = X/\cos\theta + Y\tan\theta$. (Here we make use of the fact that the convolution of two Lorentzians is a Lorentzian whose width is the sum of the individual widths. For Gaussians, the widths combine in quadrature, *i.e.*, $\Gamma^2 = \Gamma_1^2 + \Gamma_2^2$.) In the general case, where neither the instrumental response function nor the sample broadening is purely a Gaussian or Lorentzian function, one can write an empirical line shape as the approximate convolution of a Gaussian and a Lorentzian, with widths given by

$$\begin{aligned}\Gamma_G &= (U\tan^2\theta + V\tan\theta + W + P/\cos^2\theta)^{1/2},\\ \Gamma_L &= X/\cos\theta + Y\tan\theta.\end{aligned} \tag{3.2.14}$$

This is one of the flexible line-shape models available in the widely used program *GSAS* (Larson & Von Dreele, 2004). It is still possible to make a semi-quantitative statement about sample properties by comparing refined parameters against a standard sample; for example, size broadening will increase the P and X parameters, and strain will increase U and Y. A similar model is used in the *FullProf* software (Rodríguez-Carvajal, 1993, 2001; Kaduk & Reid, 2011).

3.2.3. Complications due to non-ideal sample or instrument properties

In this section, we consider various factors that modify powder X-ray diffraction data relative to the idealized situation described above.

3.2.3.1. *Absorption within a homogeneous sample*

In equations (3.2.2) and (3.2.10), it was assumed that the neither the incident nor the diffracted radiation is absorbed within the sample. However, it is generally the case that neutrons or X-rays are attenuated as they travel through any material, such that the fraction of original intensity surviving after a distance x is $I(x)/I(0) = \exp(-\mu x)$. Here μ is the linear absorption coefficient, which generally depends strongly on the composition of the sample and the X-ray wavelength.

X-ray attenuation coefficients for elements are often given as mass attenuation coefficients, μ/ρ, in units of cm^2 g^{-1}. These are available in various sources, such as *International Tables for Crystallography*, Volume C, Table 4.2.4.3, or from internet resources such as http://11bm.xray.aps.anl.gov/absorb/absorb.php. The exact positions of X-ray absorption edges can depend on the chemical environment of the atom, and so tabulated or computed atomic absorption coefficients are not entirely trustworthy within about ±100 eV of an absorption edge. The X-ray mass attenuation coefficient is related to the imaginary part of the atomic scattering factor [equation (3.2.6)] as $\mu_m = 2r_e\lambda f''/m$, where m is the atomic mass. For a compound or other mixture of elements of total density ρ in which the (dimensionless) mass fraction of element i is g_m^i, the X-ray linear absorption constant is given by

$$\mu_{\text{X-ray}} = \rho\sum_i g_m^i(\mu_m/\rho)^i.$$

In the case of neutrons used for powder diffraction, the absorption cross section is typically tabulated in barns (1 barn = 10^{-24} cm^2); see Table 4.4.4.1 in *International Tables for Crystallography*, Volume C or websites such as http://www.ncnr.nist.gov/resources/n-lengths/list.html. The neutron absorption cross section is generally inversely proportional to velocity, and values are usually tabulated for neutrons with a speed of 2200 m s^{-1} (*i.e.*, 25.3 meV kinetic energy, 1.80 Å wavelength). For neutrons, the equivalent expression with absorption cross sections depends on the number densities g_n^i (atoms/volume) of each element:

$$\mu_{\text{neutron}} = \sum_i g_n^i(\sigma_{\text{abs}}^i + \sigma_{\text{inc}}^i).$$

Considering absorption, the effective volume is given by an integral over the sample,

$$V_{\text{eff}} = \int \mathrm{d}^3\,\mathbf{R}\exp[-\mu(L_{\text{in}} + L_{\text{out}})], \tag{3.2.15}$$

where L_{in} and L_{out} are the paths of the incident and diffracted radiation to the point $\mathbf{R}$ within the sample, respectively.

The simplest case is of a sample in the form of a flat plate, with a thickness significantly greater than $1/\mu$, in the dividing position so that the angles of incidence and diffraction from the plane of the sample are both equal to θ. Let the dimensions of the beam be W in the equatorial direction (in the diffraction plane) and H in the axial direction (parallel to the diffractometer axis, *i.e.*, perpendicular to the scattering plane) as shown in Fig. 3.2.2.